Applied Catalysis B: Environmental 304 (2022) 120953

Contents lists available at ScienceDirect

Applied Catalysis B: Environmental

journal homepage: www.elsevier.com/locate/apcatb

Piezo-photocatalytic fuel cell with atomic Fe@MoS_2 on CFC helical electrode has enhanced peroxymonosulfate activation, pollutant degradation and power generation

Lin Xu [b], Lifen Liu [a,b,*]

[a] Key Lab of Industrial Ecology and Environmental Engineering, Ministry of Education, School of Ocean Science and Technology, Dalian University of Technology, 116024, Dalian, Liaoning, China

[b] Key Lab of Industrial Ecology and Environmental Engineering, Ministry of Education, School of Environmental Science and Technology, Dalian University of Technology, 116024, Dalian, Liaoning, China

ARTICLE INFO

Keywords:
Atomic Fe on MoS_2
Piezocatalysis by aeration
Piezo-Photocatalytic Fuel Cell
PMS

ABSTRACT

In this study, the catalytic performance of helical-form carbon fiber cloth anode loaded with atomic Fe@MoS_2 (Fe@MoS_2/CFC (h)) in piezocatalytic fuel cell (Pz-FC), improved 1.27 times with aeration as the piezo-driving force. The above Pz-FC with 0.5 mM peroxymonosulfate (PMS) and Xe-lamp irradiation forming a PMS-piezo-photocatalytic fuel cell (PMS-Pz-PFC) system, removed 92.8% berberine in 60 min and generated power density that were respectively 2.04-fold and 8-fold higher than the PMS-Pz-PFC using MoS_2/CFC (h) as the anode. Experiments showed that atomic Fe promoted piezo-photocatalysis of the helical-design anode significantly to accelerate the activation of PMS. Moreover, with 0.5 mM PMS, remarkable enhancement of electricity generation (more than 500 times difference) and pollutant degradation (by 40–50%) were achieved. The drastic synergy of piezoelectric catalysis in enhanced advanced oxidation has great practical application potential.

1. Introduction

Environmental pollution and energy shortage have become serious problems in the world. It is vital to find an efficient and environmental-friendly way to solve the issues [1]. Recently, as a new kind of advanced oxidation processes (AOPs), piezocatalysis has been studied for pollution control and wastewater treatment [2–4]. Piezoelectric (Pz) effect refers to the generation of the built-in electric field in the semiconductor materials with non-centrosymmetric structure during the deformation caused by mechanical forces [5]. Piezocatalysis can be used to remove pollutants driven by ultrasonic vibration or green energy resources (mechanical vibration from wind, tide, footsteps, flowing medium, etc.) [6]. It is worth mentioning that piezocatalysis can be combined with photocatalysis for more efficient degradation performance, as the built-in electric field can drive excited charge pairs to the opposite direction to accelerate the reaction rate [7]. For example, Lin et al. reported that diphasic $Ba_{0.8}Ca_{0.2}TiO_3$ nanowire could degrade MO dye completely within 40 min with the assistance of UV ultraviolet light and ultrasonic vibration [8]. However, the response of the piezocatalytic materials to mechanical forces is still not sensitive enough, thus most the existing researches using high-frequency ultrasonic disturbance as an external force, which is too complex and expensive to be applied in large-scale practice [9]. To solve the above problems, it is crucial to improve the activity of catalysts and find facile ways to provide mechanical forces.

Nowadays, lots of attention has been paid to improving piezocatalysis performance. Feng et al. prepared piezoelectric titanate (PZT) and PZT/TiO_2 catalysts with a core-shell configuration using a simple coating method, which could mineralize RhB just underwater stirring and LED irradiation [9]. Xu's team reported that barium strontium titanate (BST) particulates packaged by piezo-ceramic-polymer porous foam could efficiently purify dye wastewater with periodic low-frequency mechanical squeeze [10]. However, purely water purification can not fully meet the sustainable requirements. Recovery of chemical energy from wastewater is also of great importance in the coming carbon-neutral era.

Photocatalytic fuel cell (PFC), a system with photocatalytic electrodes, can simultaneously treat wastewater and recover energy without

* Corresponding author at: Key Lab of Industrial Ecology and Environmental Engineering, Ministry of Education, School of Ocean Science and Technology, Dalian University of Technology, 116024, Dalian, Liaoning, China.
E-mail address: lifenliu@dlut.edu.cn (L. Liu).

https://doi.org/10.1016/j.apcatb.2021.120953
Received 29 July 2021; Received in revised form 31 October 2021; Accepted 17 November 2021
Available online 20 November 2021

the extra energy input [11–13]. Inspired by PFC, it is a good choice to apply piezoelectric technology to PFC, thus piezoelectric materials can initiate mechanical deformation caused by the pressure of turbulence and bubbles rupture generated by aeration to form an inner electric field, that reduced the recombination of photo-generated electrons and improved the photocatalytic efficiency. The system with Pz materials may thus the conversion of chemical energy in pollutants to electricity assisted by mechanical energy and Pz effect, achieving the waste recycling target.

As for the preparation and activity enhancement of catalytic electrodes, some researchers used fluorine-doped tin oxide (FTO) [14–18], Ti foil [19], and Zn foil [20], etc. as the conductive substrates to in-site load the catalyst with electro-deposition or hydrothermal method. The in-situ growth method avoids the cover of active sites caused by coating and facilitates recovery of the catalysts compared with the powder form [11]. However, the high cost of substrate materials will limit the large-scale application of the system. It is a feasible way to use cheap materials instead of metal materials.

Nanoflower-like MoS_2 is considered a potential piezo-photocatalyst due to its easy-deformed layered structure, abundant edge active sites, and narrow bandgap (1.65 eV) [21,22]. It can directly grow on cheap cellulose paper by a gentle one-step hydrothermal method [23]. However, pristine MoS_2 nanoflowers do not have satisfactory piezo-photocatalytic performance due to the dependence on persistent ultrasonic disturbance and high charge recombination rate [24]. To improve the activity of MoS_2, many approaches have been put forward. Pan et al. demonstrated that fabricating MoS_2 nanosheets onto S, N-co-doped graphene could achieve excellent piezocatalytic performance, based on the acceleration effect of graphene on electron transfer [4]. From the perspective of electronic transmission acceleration, single-atom catalysts (SACs), an advanced technology with atomic economic effect, should be considered. The non-noble metal SACs, especially transition metals, have prominent research values such as oxygen reduction reaction (ORR) [25], nitrogen sensitization [26], persulfate activation [27], and H_2O_2 production [28], for its low cost and high performance. Nevertheless, little attention has been paid to the use of SACs in promoting the efficiency of piezocatalysis.

As an emerging AOPs, peroxymonosulfate (PMS) activation can produce sulfate radical ($SO_4^{\cdot-}$), which is advantageous in strong oxidation activity, wide pH range, long half-life ($t_{1/2}$ = 30–40 μs), and relatively high oxygen reduction potential (2.5–3.1 V) [29]. More importantly, studies have shown that PMS could promote the power generation performance of PFC [30]. Therefore, integrating PMS with PFC is reasonable and meaningful.

In this study, a novel piezo-photocatalytic fuel cell (Pz-PFC) with helical shaped Fe@MoS_2/CFC piezo-photocatalytic anode (Fe@MoS_2/CFC (h)) was established to treat wastewater and recover energy efficiently with PMS activation under aeration disturbance and visible light irradiation. Atomic Fe doped MoS_2 were directly grown on cheap carbon fiber cloth by a simple one-step hydrothermal method. The electrode's helical angle was fixed to 90° to promote the piezo-response sensitivity. Furthermore, a small amount of PMS was added to further improve oxidation activity of the system. Finally, the reaction mechanism of the PMS-Pz-PFC was explored by radical quenching experiments and EPR analysis. The result showed that the atomic Fe enhanced the piezo-photocatalytic performance of the system via activating PMS intensively for pollutant removal and electricity production.

2. Materials and methods

2.1. Chemicals and materials

Potassium monopersulfate triple salt (PMS), berberine chloride, and 5, 5-Dimethyl-1-pyrroline N-oxide (DMPO) were purchased from Aladdin Industrial Corporation (Shanghai, China). Sodium molybdate ($Na_2MoO_4.2\ H_2O$), thiourea (CH_4N_2S), and ferric sulfate ($Fe_2(SO_4)_3{\cdot}xH_2O$), ammonium oxalate (AO), ethanol (EtOH), tertiary butanol (TBA) were obtained from Damao Chemical Reagent Company (Tianjin, China). Carbon fiber clothes (CFCs) were made by DK Nano Technology Co., Ltd. (Beijing, China). The above reagents were all analytical grades.

2.2. Preparation of Fe@MoS_2/CFC piezo-photocatalytic helical electrode

Carbon fiber cloth (CFC, 4 cm × 9 cm) was used as the substrate, soaked in ethanol for 24 h, and washed with DI water then dried under vacuum before use. The seed solution was prepared by mixing 0.01 M of $Na_2MoO_4.2\ H_2O$ and 0.02 M of CH_4N_2S in deionized (DI) water. The pretreated carbon fiber cloth was dipped in the seed solution for 1 h followed by drying at 80 °C. The mixture containing 0.02 M of $Fe_2(SO_4)_3{\cdot}xH_2O$, 0.08 M of $Na_2MoO_4.2\ H_2O$ and 0.2 M of CH_4N_2S was stirred for 30 min. The seed-coated CFC and the mixed solution were transferred into the hydrothermal reactor and maintained at 200 °C for 20 h. After the reactor naturally cooled to room temperature, we took out the Fe@MoS_2/CFC, rinsed it with ethanol and DI three times respectively, and then put it in the oven for drying at 80 ℃. Finally, folding the Fe@MoS_2/CFC in half (the side with catalysts supported was outward), and maintaining the helical angle to 0° or twisting to 90°, then fixing them to obtain the plane-shape Fe@MoS_2/CFC electrode (Fe@MoS_2/CFC (p)) or helical-form Fe@MoS_2/CFC electrode (Fe@MoS_2/CFC (h)) respectively.

2.3. Characterization methods

The micro-morphology and microstructure of the samples were preliminarily analyzed by high-resolution transmission electron microscope (HRTEM), high-angle annular dark-field scanning transmission electron microscopy (HAADF-STEM), and energy-dispersive X-ray spectroscopy (EDS) images, captured by field emission transmission electron microscope (JEM-F200, Japan) with an accelerating voltage of 200 kV. The composition and valence of elements on the electrode were observed by X-ray photoelectron spectra (XPS, K-Alpha$^+$, UK) with Al Kα X-ray excitation source, high optimum energy resolution (≤ 0.5 eV FWHM) and optimal spatial resolution (≤ 30 μm). The related free radicals were shown by electron paramagnetic resonance spectroscopy (EPR, A200–9.5/12., Germany).

2.4. Construction and evaluation of the Pz-PFC system

A single chamber Pz-PFC using Fe@MoS_2/CFC (h) as the anode and 2 cm × 9 cm CFC as the cathode was constructed. A Xenon lamp was used as the light source, and the distance between the xenon lamp and the anode was 10 cm. Moreover, the distance between the anode and the cathode was 1 cm. The resistance of the external resistor connecting the two electrodes in the Pz-PFC was 2000 Ω, unless otherwise specified.

Berberine was chosen as the model pollutant compound (10 mg L^{-1}, 300 ml) in piezo-photocatalytic degradation tests. Before the reaction started, berberine solution was added into the Pz-PFC reactor, both Fe@MoS_2/CFC (h) and CFC cathode were immersed in the solution to reach adsorption and desorption equilibrium. After 30 min, the light and aeration were turned on, PMS was simultaneously added into the solution to initiate the oxidation reaction (PMS concentration in solution: 0.5 mM). A certain amount of samples were collected from the reactor every 10 min, the berberine concentration was determined with the characteristic absorption peak at 343 nm, using a 752 UV–Vis spectrophotometer (Shanghai Jinghua Technology Instrument Corp., China). The current-voltage plot and the current-power plot of the Pz-PFC system were measured by changing the external resistance of the system from 99,999 Ω to 1 Ω and recording the changes of the voltage using a digital multimeter (Victor VC97, China).

The reactive oxidation species (ROS) produced by the PMS-Pz-PFC were analyzed by the quenching experiments. AO, EtOH, TBA, and

nitrogen (N_2) were added to the reaction solution as trapping agents for the hole (h^+), sulfate radical ($SO_4^{\cdot-}$), hydroxyl radicals (·OH), and superoxide radicals ($\cdot O_2^-$), respectively.

3. Results and discussion

3.1. Characterizations of the Fe@MoS_2/CFC electrode

Surface chemical compositions of Fe@MoS_2/CFC were analyzed by XPS. The corresponding XPS survey spectra were shown in Fig. 1a. The region shown in Fig. 1b was for Mo 3d, the two peaks located at 228.4 eV (Mo $3d_{5/2}$) and 231.5 eV (Mo $3d_{3/2}$) belonged to Mo^{4+} in 1 T-MoS_2. Meanwhile, there were another two tiny peaks at 229.5 eV (Mo $3d_{5/2}$) and 232.5 eV (Mo $3d_{3/2}$), representing Mo^{4+} in the 2 H phase of MoS_2. In addition, the peak located at 161.2 eV was attributed to S $2p_{3/2}$ in 1 T-MoS_2, while the blue peak at 162.6 eV belonged to S $2p_{3/2}$ in 2 H-MoS_2. Furthermore, the two purple peaks at located 163.9 eV (S $2p_{3/2}$) and 165.3 eV (S $2p_{1/2}$) suggesting the introduction of Fe-S sites in Fe@MoS_2 and the higher binding energy of 167.9 eV and 169.1 eV implied that the sulfide was oxidized to sulfate as exposing in air (Fig. 1c) [31–33]. The two peaks that appeared at 707.5 eV (Fe $2p_{3/2}$) and 720.3 eV (Fe $2p_{1/2}$) confirmed that atomic Fe existed in Fe-S form in the Fe@MoS_2 [34–36]. Another two Fe $2p_{3/2}$ peaks in 710.2 eV and 714.1 eV were of Fe (II) and Fe (III), oxidized Fe species on the surface of the catalysts. (Fig. 1d) [37].

The structure morphology of catalyst Fe@MoS_2 was shown in TEM images in Fig. 2. To observe the micro-morphology, lattice structure, and elemental distribution of the Fe@MoS_2, HRTEM, HAADF-STEM, and EDS images were provided. It could be seen from Fig. 2a, the MoS_2 with nanoflower-like lamellar structure had been prepared successfully. Fig. 2b showed that a dense of bright spots (d < 0.3 nm) circled in red were well dispersed on the nanoflowers, revealing the existence of atomic Fe. The interlayer spacing of corrugations observed from Fig. 2c was 0.627 nm, corresponding to the (002) crystal plane of MoS_2 [38]. The width of the narrower lattice uniformly distributed was 0.259 nm, belonged to the (100) crystallographic plane of MoS_2 [39]. Furthermore, honeycomb patterns and hexagonal lattices existed in Fe@MoS_2 in Fig. 2d belonged to the 2 H and 1 T phase of MoS_2, respectively [40,41]. Fig. 2e-h showed that Fe elements were uniformly distributed on the Fe@MoS_2 nanoflower, further confirming the successful doping of atomic Fe.

3.2. The electricity generation performance of the Pz-PFC

The power generation capacity of the Pz-PFC using berberine (10 mg L^{-1}, 300 ml) as fuel was measured by a digital multimeter while changing the external resistance of the system from 99,999 Ω to 1 Ω during the reaction processes under different conditions. As shown in Fig. 3a-b, under the condition of aeration, illumination, and with 0.5 mM PMS, the open-circuit voltage and the short-circuit current density of the Pz-PFC (with Fe@MoS_2/CFC (h) anode and CFC cathode) (abbreviated as Fe@MoS_2/CFC (h)-CFC) were 0.325 V and 14.81 μA cm^{-2}. While the maximum power density obtained by the

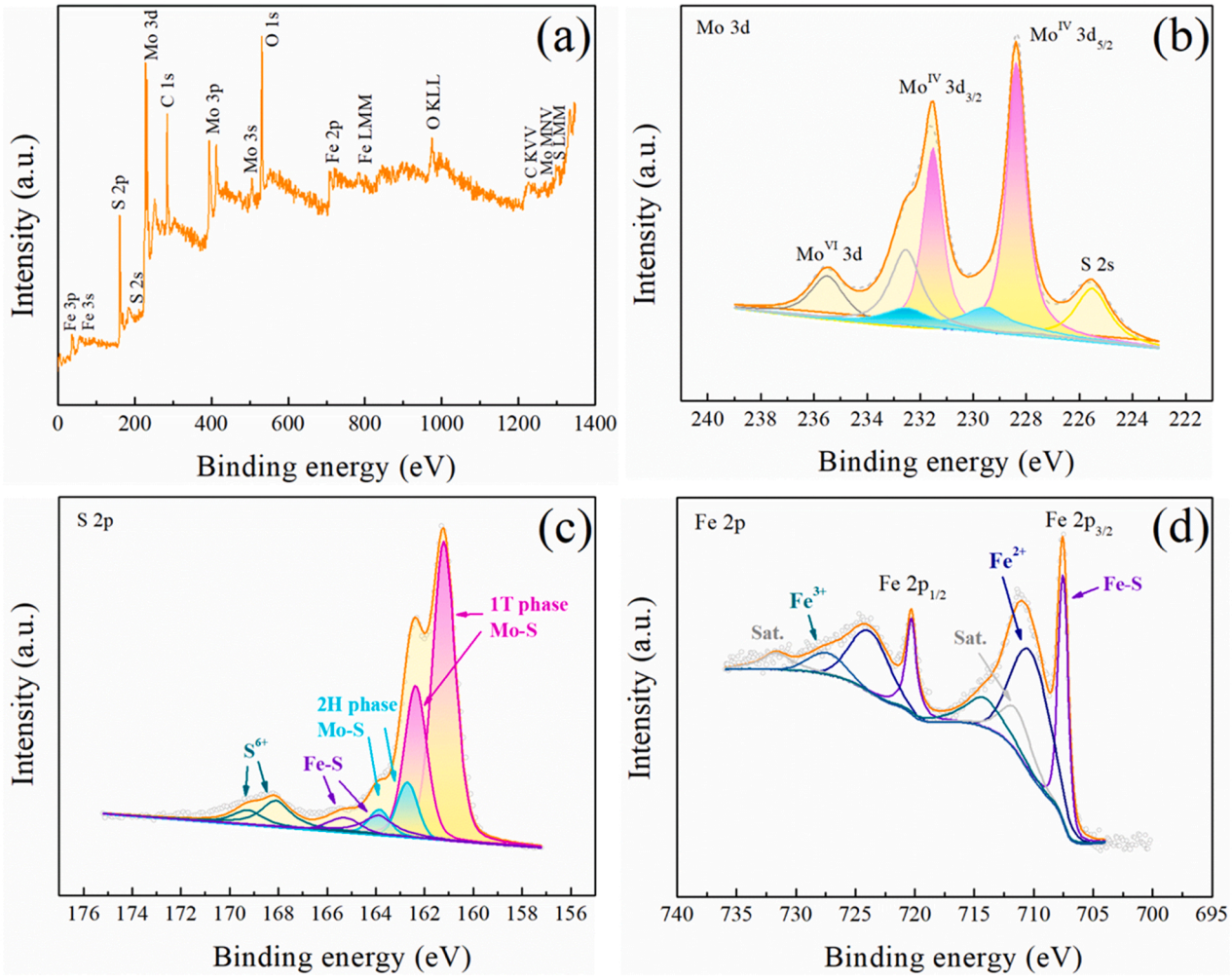

Fig. 1. Surface chemical compositions of Fe@MoS_2/CFC: (a) XPS survey spectra of Fe@MoS_2/CFC electrode; High-resolution XPS spectra of (b) Mo 3d, (c) S 2p, (d) Fe 2p.

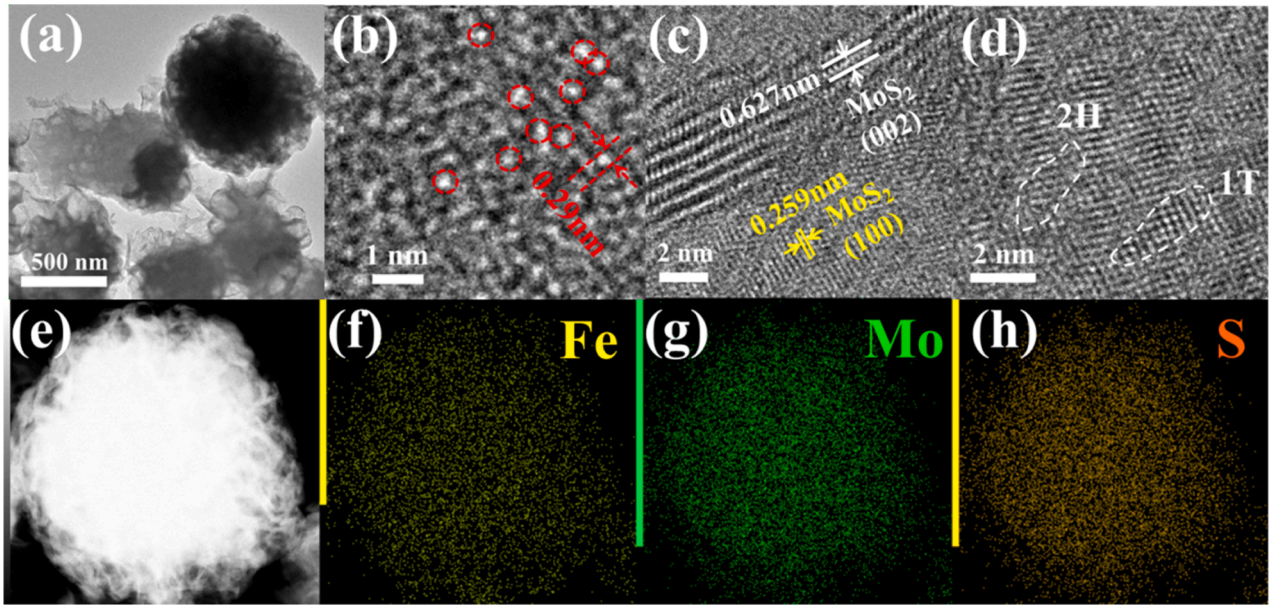

Fig. 2. Micro-morphology analysis of Fe@MoS_2: (a-d) HRTEM images, (e-h) HAADF-STEM image and the corresponding elemental mapping with scale bar = 250 nm.

system was 0.80 μW cm^{-2}.

The power density of the Fe@MoS_2/CFC (h)-CFC was decreased to 0.64 μW cm^{-2} without aeration, to 0.60 μW cm^{-2} as using plane-form anode, and to 0.30 μW cm^{-2} without light. It was only 0.0014 μW cm^{-2} if no PMS was added. (Fig. 3c). This phenomenon demonstrated that the activation of PMS was the decisive factor for electricity production. This might be because that the addition of PMS increased the electrolyte concentration, and its activation increased current density [30]. Through comparing the maximum power density with the Fe@MoS_2/CFC (h)-CFC under different conditions (no aeration 0.64 μW cm^{-2}; the plane-form anode 0.60 μW cm^{-2}, with aeration 0.80 μW cm^{-2}), it was clear to conclude that aeration could promote the electricity generation capacity of the PMS-Pz-PFC by the piezo-effect. It was worth mentioning that without light, the system energy output could still maintain at 0.30 μW cm^{-2} due to the PMS activation caused by the purely piezoelectric catalytic effect.

Experiments showed that the power density generated by Fe@MoS_2/CFC (h)-CFC (0.80 μW cm^{-2}) was 8 times higher than MoS_2/CFC (h)-CFC (0.10 μW cm^{-2}) and more than 500 times higher than the CFC (h)-CFC (0.0015 μW cm^{-2}) (Fig. 3d). It indicated that atomic Fe doping promoted the power generation capacity of the system greatly. From the above analysis, it could be inferred that the atomically dispersed Fe with abundant exposed Fe-S active sites, accelerated the transfer rates of the surface charges, promoted the separation of electrons and holes, enhanced the piezo-photocatalytic effect in activating PMS and improving the electricity generation [42].

3.3. The degradation performance of the Pz-PFC system

The Pz-PFC was established with the Fe@MoS_2/CFC (h) and CFC cathode. The catalysts loaded on the anode was 2.78 mg cm^{-2}, and that corresponded to catalysts dosage in the system at 0.33 g L^{-1} (catalyst/solution). Berberine was used as the target compound to investigate the capability of the Pz-PFC for pollutants removal. The dark adsorption was carried out for 30 min. After reaching the adsorption and desorption equilibrium, the aeration pump and xenon lamp were turned on, and PMS was added at the same time.

With only aeration disturbance, the berberine removal in Fe@MoS_2/CFC (h)-CFC system was 50% in 60 min, which was 1.27 times higher than that of MoS_2/CFC (h)-CFC (38%) (Fig. 4a). Nevertheless, the system with only CFC (h)-CFC had almost no removal ability (4%). It indicated that atomic Fe enhanced the piezocatalytic effect of nanoflower-like MoS_2 by better responding to the piezoelectric effect caused by aeration.

To further improve the degradation efficiency, piezocatalysis was integrated with photocatalysis and PMS activation. Under the joint action of aeration, light, and PMS (0.5 mM), 92.8% of berberine was removed in 60 min with Fe@MoS_2/CFC (h)-CFC, higher than that without Fe (45%) (Fig. 4b). It meant that the load of atomic Fe promoted the piezo-photocatalysis capability and accelerated the activation of PMS.

Meanwhile, the removal of berberine were 54% (no PMS) < 71% (no aeration) < 76% (no light) < 82% (planar anode) < 92% (helical anode) (Fig. 4c). The results demonstrated that PMS and aeration played key roles in the degradation process. The helical-shape design could improve the performance by increasing the turbulence and deformation pressure and stronger piezoelectric effect over the electrode. Finally, illumination also had a very positive effect on the function of the system.

In Fig. 4d, the berberine removal in the PMS-Pz-PFC under open-circuit and closed-circuit conditions, was respectively 75% and 92%, indicating that the self-bias generated between the two electrodes could speed the migration of electrons and reduce the recombination of electrons and holes to promote the efficiency.

3.4. Discussion on mechanism

The ROS in the catalytic processes is of great significance to the study of the mechanism, the radical quenching experiment is used to analyze the ROS produced by the PMS-Pz-PFC. After adding AO, EtOH, TBA and N_2 respectively to the reactor to quench h^+, $SO_4^{\cdot-}$,·OH, and $O_2^{\cdot-}$, the degradation of berberine was decreased from 92% to 46%, 54%, 68% and 75% shown as Fig. 5a. This phenomenon indicated that the h^+ and $SO_4^{\cdot-}$ were the dominant factors in the reaction, while·OH and $O_2^{\cdot-}$ also counted for the degradation reaction but to a less degree. Combining the above experiments with previous studies [30,43], the feasible mechanism of this experiment was summarized as follows (Eqs. (1–12)).

When mechanical force and light acted on the Fe@MoS_2/CFC (h) anode, the electrons (e^-) and holes (h^+) produced by piezo-photocatalysis migrated in the opposite direction to the surface of the material (Eq. (1)) driven by the built-in electric field. The piezo-photo

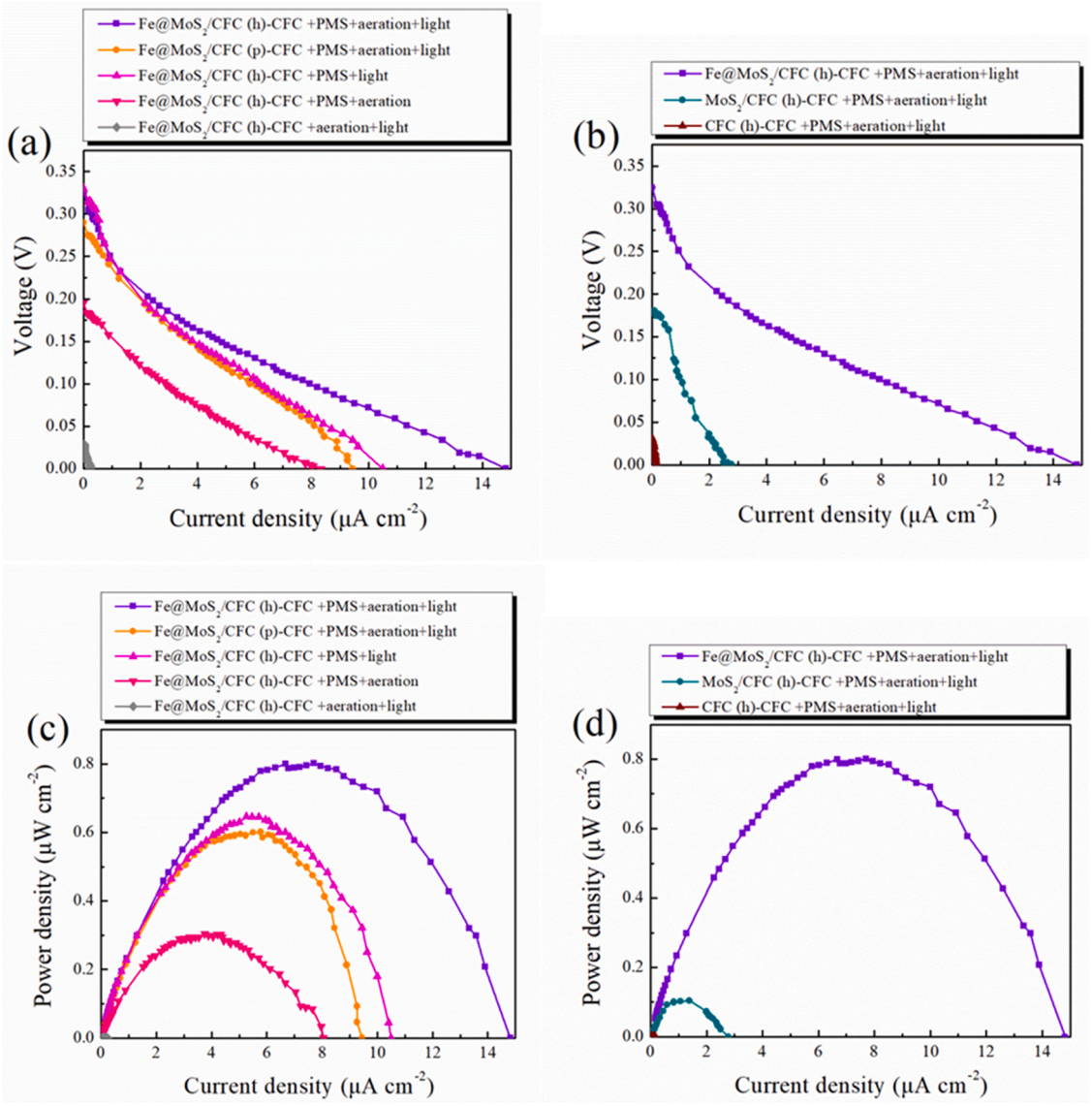

Fig. 3. Evaluation of power generation capacity of the system: (a) current-voltage plot and (c) current-power plot for the Fe@MoS_2/CFC-CFC in different conditions (with Fe@MoS_2/CFC (h) or Fe@MoS_2/CFC (p) as anode; the Fe@MoS_2/CFC (h)-CFC without PMS, without aeration and without light); (b) the current-voltage plot and (d) current-power plot of Fe@MoS_2/CFC (h)-CFC, MoS_2/CFC (h)-CFC and CFC (h)-CFC systems with 10 mg L^{-1} berberine as fuel and adding 0.5 mM PMS under aeration and illumination.

generated holes oxidized H_2O/OH^- to·OH (Eqs. (2) and (3)). The electrons were transferred through the external circuit to the cathode and reacted with oxygen and proton to form a series of strong oxidizing substances ($O_2^{\cdot-}$,·OH, H_2O_2, etc.) (Eqs. (4–7)). With the addition of PMS, a large number of $SO_4^{\cdot-}$ and·OH were produced, which greatly improved the oxidation performance of the Pz-PFC. (Eqs. (8–11)). Finally, the refractory organic pollutants were mineralized by the above active species referred to Eq. (12).

Pz-PFC:

$$Fe@MoS_2/CFC\ (h) + \text{mechanical force} + h\nu \rightarrow Fe@MoS_2/CFC\ (h)\ (e^- + h^+) \quad (1)$$

$$H_2O + h^+ \rightarrow H^+ + \cdot OH \quad (2)$$

$$OH^- + h^+ \rightarrow \cdot OH \quad (3)$$

$$O_2 + e^- \rightarrow O_2^{\cdot-} \quad (4)$$

$$O_2^{\cdot-} + 2H_2O + e^- \rightarrow 2\cdot OH + 2OH^- \quad (5)$$

$$2H^+ + O_2 + 2e^- \rightarrow H_2O_2 \quad (6)$$

$$\cdot OH + H_2O_2 \rightarrow H^+ + H_2O + O_2^{\cdot-} \quad (7)$$

PMS-Pz-PFC:

$$HSO_5^- + e^- \rightarrow SO_4^{\cdot-} + OH^- \quad (8)$$

$$HSO_5^- + e^- \rightarrow SO_4^{2-} + \cdot OH \quad (9)$$

$$HSO_5^- + h^+ \rightarrow SO_5^{\cdot-} + H^+ \quad (10)$$

$$SO_4^{\cdot-} + OH^- \rightarrow \cdot OH + SO_4^{2-} \quad (11)$$

Degradation process:

$$\text{Berberine} + h^+/SO_4^{\cdot-}/OH/O_2^{\cdot-} \rightarrow \text{products} \quad (12)$$

To further explore the ability of each system to produce ROS, EPR analyses were performed. As shown in Fig. 5b, the PMS-Pz-PFC with Fe@MoS_2/CFC (h) anode had the strongest signal peaks belonged to·OH

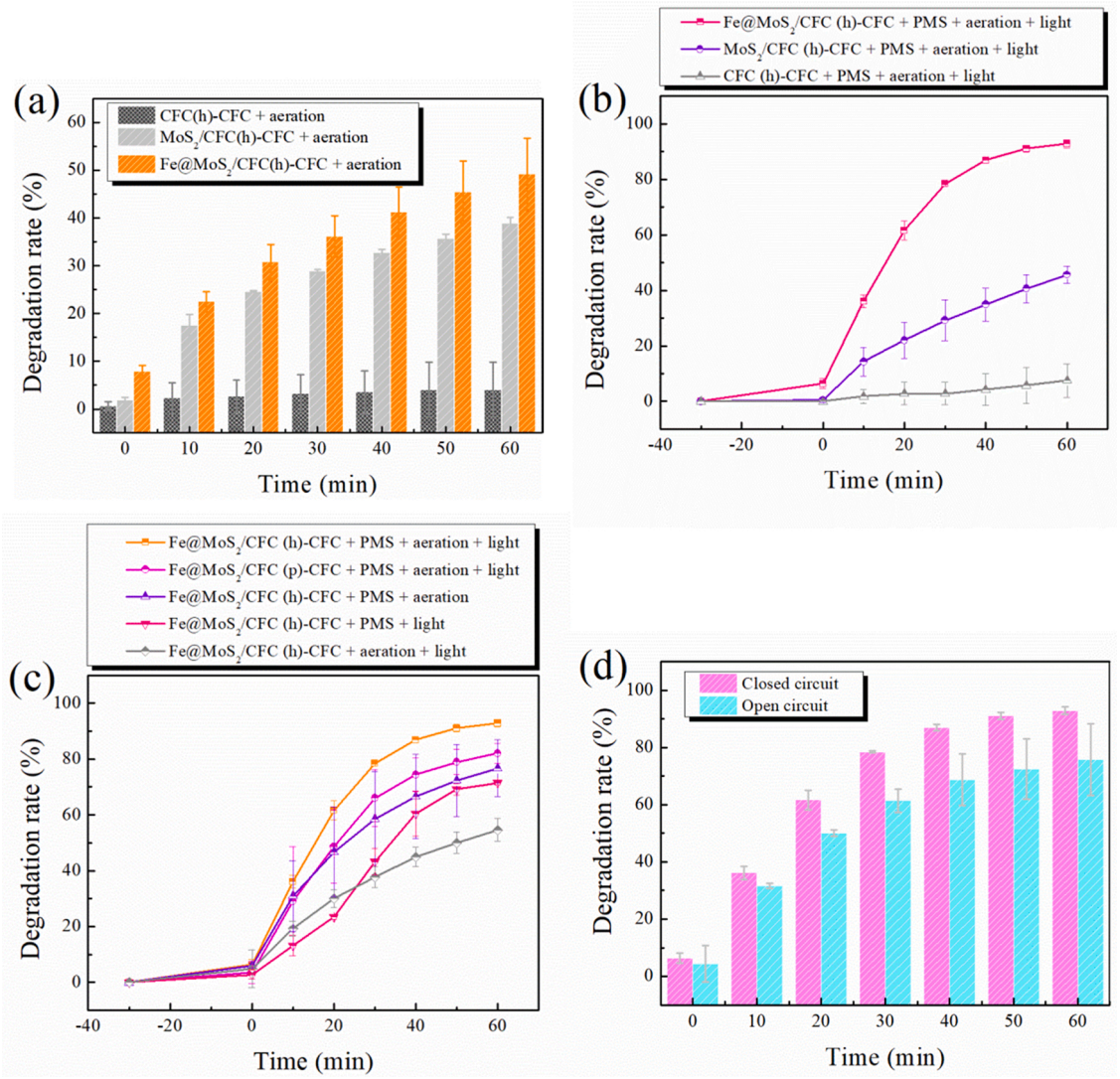

Fig. 4. The degradation performance of the fuel cells using 10 mg L^{-1} berberine as fuel under different conditions: (a) Fe@MoS_2/CFC (h)-CFC, MoS_2/CFC (h)-CFC and CFC (h)-CFC under only aeration and (b) the joint action of aeration, light and PMS (0.5 mM) conditions. (c) Fe@MoS_2/CFC-CFC under the conditions of no PMS, no aeration, no light, planar electrode, and helical electrode. (d) The PMS-Pz-PFC under open-circuit and closed-circuit conditions with Fe@MoS_2/CFC (h) as anode and CFC as cathode.

and $SO_4^{\cdot-}$ [44–46]. It means that Fe doped anode has the best catalytic performance, which is consistent with the above conclusion. When turning off the light, the Pz-FC can still activate PMS to produce strong signals (Fig. 5c). It demonstrated that Fe@MoS_2/CFC (h) anode has excellent piezoelectric effects.

Considering the above experimental results (3.2, 3.3, and 3.4), it was speculated that doping of atomic Fe on MoS_2 could improve the piezo-photocatalytic activity of the catalysts, and promote the capability of PMS activation. From Tables S1 and S2, the same could be concluded through the comparisons with other reaction rate constant (k), reaction time, and treatment capacity.

3.5. Recycling performance

To evaluate the durability and stability of the PMS-Pz-PFC, the system was run continuously for four cycles. As depicted in Fig. 6, in the fourth cycle, the degradation rate only decreases by 5%, which might be due to the decrease of active sites caused by a small amount of catalyst shedding. This shows that the system has good recycling ability.

4. Conclusions

In this study, excellent PMS activation, pollutant degradation and power generation efficiency were achieved using helical-form carbon fiber cloth piezo-photocatalytic anode loaded with MoS_2 and atomic Fe, in the PMS-Pz-PFC system. The electrode has better piezoelectric responses to the mechanical force produced by aeration, and thus higher catalytic activity. The PMS-Pz-PFC system, with aeration as the piezo-driving force, light irradiation from Xe lamp and 0.5 mM PMS, had significantly improved performance in berberine degradation (92.8%, 60 min) and power generation (0.80 μW cm^{-2}). The power density of the PMS-Pz-PFC was only 0.0014 μW cm^{-2} without PMS, was 0.30 μW cm^{-2} without light irradiation, was 0.60 μW cm^{-2} with the plane-shape anode, and 0.64 μW cm^{-2} if no aeration was applied. While the berberine removal of the PMS-Pz-PFC was respectively 54% (no PMS), 71% (no aeration), and 76% (no light), it was 82% when the anode was planar and 92.8% when the anode was helical.

This PMS-Pz-PFC system means great progress in the field of AOPs, because it can use energy from turbulence (from aeration or waves) and sunlight etc. synergistically, achieving high efficiency and low energy consumption, has broad practical application prospects.

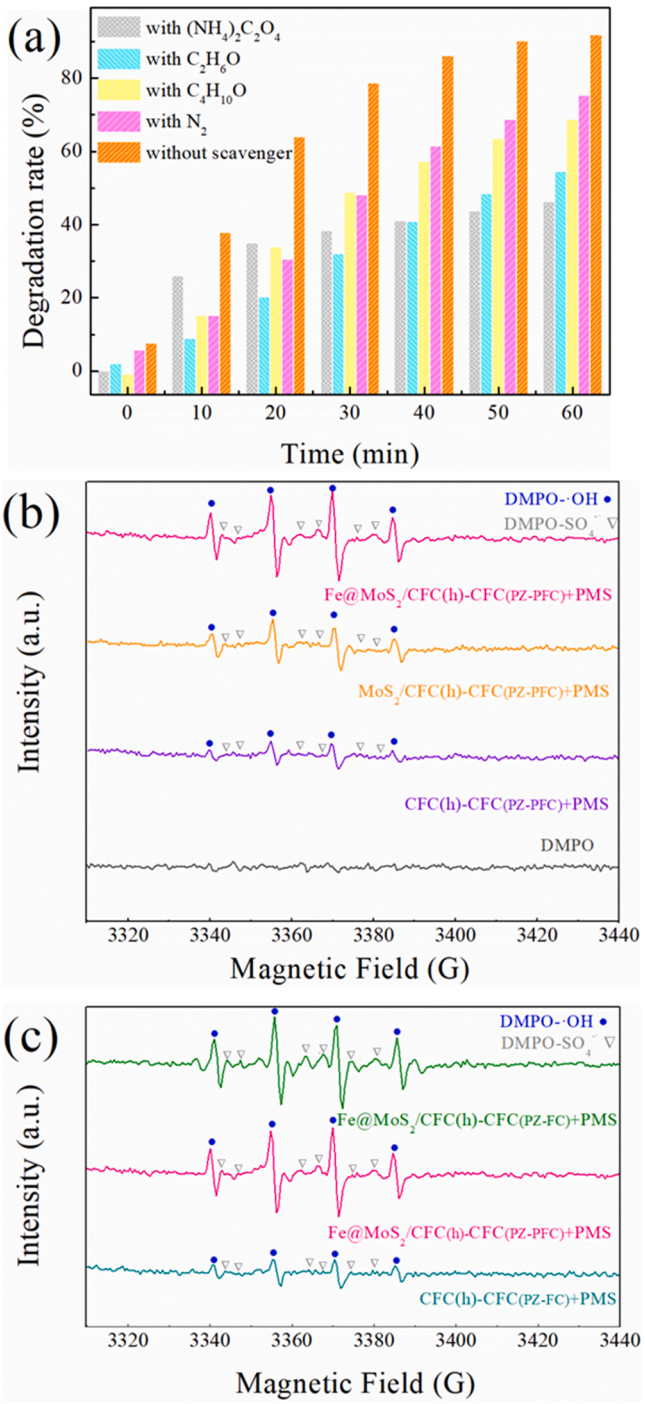

Fig. 5. Radical quenching and EPR analysis: (a) the effect of different quenching agents on the removal of 10 mg L^{-1} berberine in the PMS-Pz-PFC (Fe@MoS_2/CFC (h)-CFC) under aeration, illumination and 0.5 mM PMS. (b) EPR spectra of $SO_4^{·-}$ and·OH signal in the PMS-Pz-PFC (Fe@MoS_2/CFC (h)-CFC, MoS_2/CFC (h)-CFC, CFC (h)-CFC) or (c) the PMS-Pz-FC (Fe@MoS_2/CFC (h)-CFC, CFC (h)-CFC) with 0.5 mM PMS, using DMPO as the spin-trapping agent.

CRediT authorship contribution statement

L. Liu supervised the project and conceived the original ideas. L. Xu designed, carried out the experiments and wrote the manuscript, L. Liu revised the manuscript.

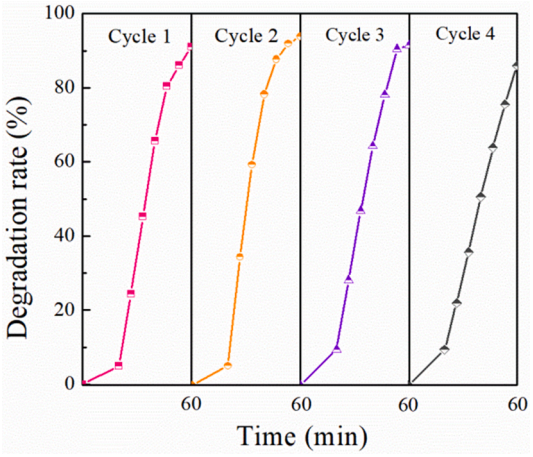

Fig. 6. Recycling runs of the berberine degradation (10 mg L^{-1}) in the Fe@MoS_2/CFC (h)-CFC with 0.5 mM PMS, aeration and light.

Declaration of Competing Interest

The authors declare that they have no known competing financial interests or personal relationships that could have appeared to influence the work reported in this paper.

Acknowledgements

Authors acknowledge the financial support from The Committee of China National Natural Science Foundation, Project (No. 21677025).

Appendix A. Supporting information

Supplementary data associated with this article can be found in the online version at doi:10.1016/j.apcatb.2021.120953.

References

[1] Y. Zeng, N. Guo, H. Li, Q. Wang, X. Xu, Y. Yu, X. Han, H. Yu, Construction of flower-like $MoS_2/Ag_2S/Ag$ Z-scheme photocatalysts with enhanced visible-light photocatalytic activity for water purification, Sci. Total Environ. 659 (2019) 20–32, https://doi.org/10.1016/j.scitotenv.2018.12.333.
[2] A. Biswas, S. Saha, N.R. Jana, $ZnSnO_3$ Nanoparticle-Based Piezocatalysts for Ultrasound-Assisted Degradation of Organic Pollutants, ACS Appl. Nano Mater. 2 (2019) 1120–1128, https://doi.org/10.1021/acsanm.9b00107.
[3] K.-S. Hong, H. Xu, H. Konishi, X. Li, Piezoelectrochemical Effect: A New Mechanism for Azo Dye Decolorization in Aqueous Solution through Vibrating Piezoelectric Microfibers, J. Phys. Chem. C. 116 (2012) 13045–13051, https://doi.org/10.1021/jp211455z.
[4] M. Pan, S. Liu, J.W. Chew, Unlocking the high redox activity of MoS_2 on dual-doped graphene as a superior piezocatalyst, Nano Energy 68 (2020), 104366, https://doi.org/10.1016/j.nanoen.2019.104366.
[5] P. Wang, X. Li, S. Fan, X. Chen, M. Qin, D. Long, M.O. Tadé, S. Liu, Impact of Oxygen Vacancy Occupancy on Piezo-catalytic Activity of $BaTiO_3$ nanobelt, Appl. Catal. B 279 (2020), 119340, https://doi.org/10.1016/j.apcatb.2020.119340.
[6] M. Pan, C. Zhang, J. Wang, J.W. Chew, G. Gao, B. Pan, Multifunctional Piezoelectric Heterostructure of $BaTiO_3$ @ Graphene: Decomplexation of Cu-EDTA and Recovery of Cu, Environ. Sci. Technol. 53 (2019) 8342–8351, https://doi.org/10.1021/acs.est.9b02355.
[7] X. Xue, W. Zang, P. Deng, Q. Wang, L. Xing, Y. Zhang, Z.L. Wang, Piezo-potential enhanced photocatalytic degradation of organic dye using ZnO nanowires, Nano Energy 13 (2015) 414–422, https://doi.org/10.1016/j.nanoen.2015.02.029.
[8] E. Lin, J. Wu, N. Qin, B. Yuan, Z. Kang, D. Bao, Enhanced piezocatalytic, photocatalytic and piezo-/photocatalytic performance of diphasic $Ba_{1x}Ca_xTiO_3$ nanowires near a solubility limit, Catal. Sci. Technol. 9 (2019) 6863–6874, https://doi.org/10.1039/C9CY01713E.
[9] Y. Feng, H. Li, L. Ling, S. Yan, D. Pan, H. Ge, H. Li, Z. Bian, Enhanced Photocatalytic Degradation Performance by Fluid- Induced Piezoelectric Field, Environ. Sci. Technol. 52 (2018) 7842–7848, https://doi.org/10.1021/acs.est.8b00946.
[10] S. Xu, W. Qian, D. Zhang, X. Zhao, X. Zhang, C. Li, C.R. Bowen, Y. Yang, A coupled photo-piezo-catalytic effect in a BST-PDMS porous foam for enhanced dye wastewater degradation, Nano Energy 77 (2020), 105305, https://doi.org/10.1016/j.nanoen.2020.105305.

[11] Y. Zhang, L. Liu, B. Van der Bruggen, M.K.H. Leung, F. Yang, A free-standing 3D nano-composite photo-electrode-Ag/ZnO nanorods arrays on Ni foam effectively degrade berberine, Chem. Eng. J. 373 (2019) 179–191, https://doi.org/10.1016/j.cej.2019.05.026.
[12] Z. Wu, G. Zhao, Y. Zhang, J. Liu, Y.-n Zhang, H. Shi, A solar-driven photocatalytic fuel cell with dual photoelectrode for simultaneous wastewater treatment and hydrogen production, J. Mater. Chem. A 3 (2015) 3416–3424, https://doi.org/10.1039/C4TA06604A.
[13] J. Zhang, J. Zheng, W. Yang, Green supercapacitor assisted photocatalytic fuel cell system for sustainable hydrogen production, Chem. Eng. J. 403 (2020), 126368, https://doi.org/10.1016/j.cej.2020.126368.
[14] D. Chen, Z. Liu, S. Zhang, Enhanced PEC performance of hematite photoanode coupled with bimetallic oxyhydroxide NiFeOOH through a simple electroless method, Appl. Catal. B 265 (2019), 118580, https://doi.org/10.1016/j.apcatb.2019.118580.
[15] J. Liu, J. Li, Y. Li, J. Guo, S.-M. Xu, R. Zhang, M. Shao, Photoelectrochemical water splitting coupled with degradation of organic pollutants enhanced by surface and interface engineering of $BiVO_4$ photoanode, Appl. Catal. B 278 (2020), 119268, https://doi.org/10.1016/j.apcatb.2020.119268.
[16] T. Zhu, Y. Liang, Y. Wang, J. Wang, W. Wang, J. Fu, L. Yao, Y. Cheng, H. Han, P-type β-$Ni(OH)_2$ nanoparticles sensitize CdS nanorod array photoanode to prolong charge carrier lifetime and highly improve bias-free visible-light-driven H_2 evaluation, Appl. Catal. B 271 (2020), 118945, https://doi.org/10.1016/j.apcatb.2020.118945.
[17] Y. Zhang, Y. Bu, F. Jiang, H. Li, X. Chen, J.-P. Ao, Mechanism on $BiVO_4$ photoanode photoelectrochemical performance improving: Based on surface electrochemical reduction method, Electrochim. Acta 366 (2021), 137288, https://doi.org/10.1016/j.electacta.2020.137288.
[18] T. Zhou, S. Chen, L. Li, J. Wang, Y. Zhang, Carbon quantum dots modified anatase/rutile TiO_2 photoanode with dramatically enhanced photoelectrochemical performance, Appl. Catal. B 269 (2020), 118776, https://doi.org/10.1016/j.apcatb.2020.118776.
[19] D. Wang, Y. He, N. Zhong, Z. He, Y. Shen, T. Zeng, X. Lu, J. Ma, S. Song, In situ chloride-mediated synthesis of TiO_2 thin film photoanode with enhanced photoelectrochemical activity for carbamazepine oxidation coupled with simultaneous cathodic H_2 production and CO_2 conversion to fuels, J. Hazard. Mater. 410 (2020), 124563, https://doi.org/10.1016/j.jhazmat.2020.124563.
[20] Q. Shi, M. Zhang, Z. Zhang, Y. Li, Y. Qu, Z. Liu, J. Yang, M. Xie, W. Han, Energy and separation optimization of photogenerated charge in $BiVO_4$ quantum dots by piezo-potential for efficient gaseous pollutant degradation, Nano Energy 69 (2020), 104448, https://doi.org/10.1016/j.nanoen.2020.104448.
[21] J.M. Wu, Y.-G. Sun, W.-E. Chang, J.-T. Lee, Piezoelectricity induced water splitting and formation of hydroxyl radical from active edge sites of MoS_2 nanoflowers, Nano Energy 46 (2018) 372–382, https://doi.org/10.1016/j.nanoen.2018.02.010.
[22] F. Guo, X. Huang, Z. Chen, H. Ren, M. Li, L. Chen, MoS_2 nanosheets anchored on porous $ZnSnO_3$ cubes as an efficient visible-light-driven composite photocatalyst for the degradation of tetracycline and mechanism insight, J. Hazard. Mater. 390 (2020), 122158, https://doi.org/10.1016/j.jhazmat.2020.122158.
[23] P.T. Gomathi, P. Sahatiya, S. Badhulika, Large-Area, Flexible Broadband Photodetector Based on ZnS-MoS_2 Hybrid on Paper Substrate, Adv. Funct. Mater. 27 (2017), 1701611, https://doi.org/10.1002/adfm.201701611.
[24] X. Zhao, Y. Lei, P. Fang, H. Li, Q. Han, W. Hu, C. He, Piezotronic effect of single/few-layers MoS_2 nanosheets composite with TiO_2 nanorod heterojunction, Nano Energy 66 (2019), 104168, https://doi.org/10.1016/j.nanoen.2019.104168.
[25] H. Yang, Z. Li, S. Kou, G. Lu, Z. Liu, A Complex-Sequestered Strategy to Fabricate Fe Single-atom Catalyst for Efficient Oxygen Reduction in a Broad pH-range, Appl. Catal. B 278 (2020), 119270, https://doi.org/10.1016/j.apcatb.2020.119270.
[26] T. Hou, H. Peng, Y. Xin, S. Wang, W. Zhu, L. Chen, Y. Yao, W. Zhang, S. Liang, L. Wang, Fe Single-Atom Catalyst for Visible-Light Driven Photofixation of Nitrogen Sensitized by Triphenylphosphine and Sodium Iodide, ACS Catal. 10 (2020) 5502–5510, https://doi.org/10.1021/acscatal.0c00920.
[27] L.-Z. Huang, C. Zhou, M. Shen, E. Gao, C. Zhang, X.-M. Hu, Y. Chen, Y. Xue, Z. Liu, Persulfate activation by two-dimensional MoS_2 confining single Fe atoms: Performance, mechanism and DFT calculations, J. Hazard. Mater. 389 (2020), 122137, https://doi.org/10.1016/j.jhazmat.2020.122137.
[28] Z. Teng, W. Cai, W. Sim, Q. Zhang, C. Wang, C. Su, T. Ohno, Photoexcited single metal atom catalysts for heterogeneous photocatalytic H_2O_2 production: Pragmatic guidelines for predicting charge separation, Appl. Catal. B 282 (2020), 119589, https://doi.org/10.1016/j.apcatb.2020.119589.
[29] L. Wang, J. Di, J. Nie, G. Ma, Multicomponent Doped Sugar-Coated Nanofibers for Peroxymonosulfate Activation, ACS Appl. Nano Mater. 2 (2019) 6998–7007, https://doi.org/10.1021/acsanm.9b01505.
[30] Y. Zhang, L. Liu, Q. Chen, Y. He, M.K.H. Leung, Electricity generating & high efficiency advanced oxidation process including peroxymonosulfate activation in photocatalytic fuel cell, Chem. Eng. J. 378 (2019), 122148, https://doi.org/10.1016/j.cej.2019.122148.
[31] F. Meng, W. Ma, Y. Wang, Z. Zhu, Z. Chen, G. Lu, A tribo-positive Fe@MoS_2 piezocatalyst for the durable degradation of tetracycline: degradation mechanism and toxicity assessment, Environ. Sci.: Nano 7 (2020) 1704–1718, https://doi.org/10.1039/D0EN00284D.
[32] B. Tang, Z.G. Yu, H.L. Seng, N. Zhang, X. Liu, Y.-W. Zhang, W. Yang, H. Gong, Simultaneous edge and electronic control of MoS_2 nanosheets through Fe doping for an efficient oxygen evolution reaction, Nanoscale 10 (2018) 20113–20119, https://doi.org/10.1039/C8NR06659K.
[33] Y. Xin, Z. Li, W. Wu, B. Fu, Z. Zhang, Pyrite FeS_2 Sensitized TiO_2 Nanotube Photoanode for Boosting Near-Infrared Light Photoelectrochemical Water Splitting, ACS Sustain, Chem. Eng. 4 (2016) 6659–6667, https://doi.org/10.1021/acssuschemeng.6b01533.
[34] L.-Z. Huang, X. Wei, E. Gao, C. Zhang, X.-M. Hu, Y. Chen, Z. Liu, N. Finck, J. Lützenkirchen, D.D. Dionysiou, Single Fe atoms confined in two-dimensional MoS_2 for sulfite activation: A biomimetic approach towards efficient radical generation, Appl. Catal. B 268 (2020), 118459, https://doi.org/10.1016/j.apcatb.2019.118459.
[35] Y. Li, S. Zhu, Y. Xu, R. Ge, J. Qu, M. Zhu, Y. Liu, J.M. Cairney, R. Zheng, S. Li, J. Zhang, W. Li, FeS_2 bridging function to enhance charge transfer between MoS_2 and g-C_3N_4 for efficient hydrogen evolution reaction, Chem. Eng. J. 421 (2021), 127804, https://doi.org/10.1016/j.cej.2020.127804.
[36] S. Choi, C. Kim, J.Y. Lee, T.H. Lee, K.C. Kwon, S. Kang, S.A. Lee, K.S. Choi, J. M. Suh, K. Hong, S.E. Jun, W.K. Kim, S.H. Ahn, S. Han, S.Y. Kim, C.-H. Lee, H. W. Jang, Vertically aligned MoS_2 thin film catalysts with Fe-Ni sulfide nanoparticles by one-step sulfurization for efficient solar water reduction, Chem. Eng. J. 418 (2021), 129369, https://doi.org/10.1016/j.cej.2021.129369.
[37] G. Gan, X. Li, L. Wang, S. Fan, J. Mu, P. Wang, G. Chen, Active Sites in Single-Atom Fe-N_x-C Nanosheets for Selective Electrochemical Dechlorination of 1,2-Dichloroethane to Ethylene, ACS Nano 14 (2020) 9929–9937, https://doi.org/10.1021/acsnano.0c02783.
[38] X. Zhao, X. Zhang, Z. Xue, W. Chen, Z. Zhou, T. Mu, Fe nanodot-decorated MoS_2 nanosheets on carbon cloth: an efficient and flexible electrode for ambient ammonia synthesis, J. Mater. Chem. A 7 (2019) 27417–27422, https://doi.org/10.1039/C9TA09264A.
[39] P. Wang, J. Zhang, G. Wang, B. Duan, D. He, T. Wang, F. Li, Synthesis and characterization of MoS_2/Fe@Fe_3O_4 nanocomposites exhibiting enhanced microwave absorption performance at normal and oblique incidences, J. Mater. Sci. Technol. 35 (2019) 1931–1939, https://doi.org/10.1016/j.jmst.2019.05.021.
[40] Y.-T. Lin, S.-N. Lai, J.M. Wu, Simultaneous Piezoelectrocatalytic Hydrogen-Evolution and Degradation of Water Pollutants by Quartz Microrods@Few-Layered MoS_2 Hierarchical Heterostructures, Adv. Mater. 32 (2020), 2002875, https://doi.org/10.1002/adma.202002875.
[41] Y.-J. Chung, C.-S. Yang, J.-T. Lee, G.H. Wu, J.M. Wu, Coupling Effect of Piezo–Flexocatalytic Hydrogen Evolution with Hybrid 1T- and 2H-Phase Few-Layered $MoSe_2$ Nanosheets, Adv. Energy Mater. 10 (2020), 2002082, https://doi.org/10.1002/aenm.202002082.
[42] F. Zhang, Y. Zhu, Q. Lin, L. Zhang, X. Zhang, H. Wang, Noble-metal single-atoms in thermocatalysis, electrocatalysis, and photocatalysis, Energy Environ. Sci. 14 (2021) 2954–3009, https://doi.org/10.1039/D1EE00247C.
[43] S. Lan, Y. Chen, L. Zeng, H. Ji, W. Liu, M. Zhu, Piezo-activation of peroxymonosulfate for benzothiazole removal in water, J. Hazard. Mater. 393 (2020), 122448, https://doi.org/10.1016/j.jhazmat.2020.122448.
[44] Y. Zong, X. Guan, J. Xu, Y. Feng, Y. Mao, L. Xu, H. Chu, D. Wu, Unraveling the Overlooked Involvement of High-Valent Cobalt-Oxo Species Generated from the Cobalt(II)-Activated Peroxymonosulfate Process, Environ. Sci. Technol. 54 (2020) 16231–16239, https://doi.org/10.1021/acs.est.0c06808.
[45] Y. Gao, Y. Zhu, T. Li, Z. Chen, Q. Jiang, Z. Zhao, X. Liang, C. Hu, Unraveling the High-Activity Origin of Single-Atom Iron Catalysts for Organic Pollutant Oxidation via Peroxymonosulfate Activation, Environ. Sci. Technol. 55 (2021) 8318–8328, https://doi.org/10.1021/acs.est.1c01131.
[46] T. Chen, Z. Zhu, H. Zhang, Y. Qiu, D. Yin, G. Zhao, Facile Construction of a Copper-Containing Covalent Bond for Peroxymonosulfate Activation: Efficient Redox Behavior of Copper Species via Electron Transfer Regulation, ACS Appl. Mater. Interfaces 12 (2020) 42790–42802, https://doi.org/10.1021/acsami.0c11268.